A Novel Ring-shaped Extensional Wine-glass Mode RF-MEMS Resonator with High Quality Factors

Zeji Chen*, Wenli Liu*, Quan Yuan, Yinfang Zhu, Jinling Yang, and Fuhua Yang
Institute of Semiconductors, Chinese Academy of Sciences
Beijing, P. R. China
yfzhu@semi.ac.cn, and jlyang@semi.ac.cn

Zeji Chen*, Wenli Liu*, Quan Yuan, Yinfang Zhu, Jinling Yang, and Fuhua Yang
The Center of Materials Science and Optoelectronics Engineering, University of Chinese Academy of Sciences
Beijing, P. R. China

Zeji Chen*, Wenli Liu*, Quan Yuan, Yinfang Zhu, and Jinling Yang
The State Key Laboratory of Transducer Technology
Shanghai, P. R. China
*These authors contributed equally to this work

***Abstract*—This work presents a novel extensional wine-glass mode (EWGM) resonator with high *Q* values. For the first time, a flexible straight beam-frame mixing tether design was proposed, which simultaneously reduces the mechanical stiffness and optimizes the strain energy distribution. Contrast to conventional ultra-high frequency (UHF) devices suffering from severe anchor loss and high bias voltages, the proposed device exhibits superior performance. With frequency up to 548.19 MHz, the resonator can be driven into vibrations using a low bias voltage down to 7 V, while an excellent *Q* over 1.5 × 10^4 was implemented.**

Keywords—anchor loss; extensional wine-glass mode; MEMS resonator; quality factor.

I. INTRODUCTION

Future wireless communications feature large capacity, high data rate, multi-band, and reconfigurability [1, 2]. Radio frequency micro-electro-mechanical system (RF-MEMS) resonators with IC compatibility, small size, and low power consumption have emerged as essential devices [3]. To meet the fast-growing demands of higher operating frequencies, MEMS resonators with high *Q* values vibrating at ultra-high frequency (UHF) ranges are extremely desired [4, 5]. Various advanced RF modules, such as high frequency oscillators free of phase lock loops (PLL) [6], and ultra-narrow passband filters for RF channel selections [7], are based on high-performance UHF resonators. However, there still exist two significant issues that restrict the viable applications of such devices.

Firstly, maintaining high *Q* values at UHF range is still a bottleneck for state-of-art MEMS resonators. The anchor loss contributes most to the energy dissipations. Limited by the fabrication tolerances, it is generally hard to proportionally scale down the supporting structures with the resonating body, therefore, the widely-used routine to attain high frequencies is to excite the high-order modes. Nevertheless, with larger motions in the vicinity of the supporting structures, the anchor loss tends to be more significant. For instance, the *Q* of contour mode resonator reduces from 23000 at 193.2 MHz in the fundamental mode to undetectable at 829.6 MHz in the 3rd mode [8]. For width extensional mode (WEM) resonators, the *Q* values of the even modes are severely degraded since the supporting tethers are subject to the maximum displacements [9].

In addition, due to the greatly increased stiffness, higher DC bias voltages (V_P) are required, which imposes an obstacle against the integration of MEMS resonators with CMOS circuits. For instance, to excite the 3rd WEM, high bias voltages up to 60 V was required [9]. An alternative method is to use mixing measurement scheme. Despite the suppressed feedthrough signals, the driving/sensing configurations are complicated, besides, local oscillator signal still requires high amplitudes [10].

In this work, a novel ring-shaped extensional wine-glass mode (EWGM) resonator was exploited. A beam-frame mixing supporting tether was developed, which simultaneously enables optimal strain energy distributions and reduced mechanical stiffness. Hereby superior *Q* values and substantially reduced bias voltages were achieved.

II. RESONATOR DESIGN

A. Mode properties

The mode shape of EWGM is given in Fig. 1. As can be seen, four quasi nodal points are uniformly distributed along the circumference. The outer and inner perimeters within the quarter ring are expanding or contracting in phase, while two adjacent quarter rings exhibit anti-phase vibrations. The radial displacement profile of EWGM can be depicted via the following expression [11]:

$$u_r = \frac{1}{h}\left(A\frac{dJ_2(hr)}{dr} + B\frac{dY_2(hr)}{dr} + \frac{2}{r}\left(CJ_2(kr) + DY_2(kr)\right)\right)\cos 2\theta \cdot e^{j\omega_0 t}, \quad (1)$$

where r and θ are polar coordinates, A, B, C, and D are constants, ω_0 denotes the angular resonance frequency, k and h are frequency-dependent parameters which have the relation as:

978-1-6654-3935-0/21/$31.00 ©2021 IEEE

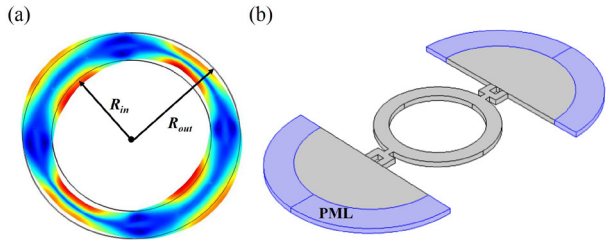

Fig. 1. The displacement profile of the EWGM (a) and the FEA model for mechanical stiffness extraction and Qanchor calculation.

$$\frac{h}{k}=\frac{1-\nu}{2}, \tag{2}$$

where v refers to the Poisson's ratio. For EWGM resonators, the boundaries conditions take the forms as [12]:

$$\begin{aligned} T_{rr}\big|_{r=R_{in}}&=0,\ T_{rr}\big|_{r=R_{out}}=0,\\ T_{r\theta}\big|_{r=R_{in}}&=0,\ T_{r\theta}\big|_{r=R_{out}}=0, \end{aligned} \tag{3}$$

where T_{rr} and $T_{r\theta}$ are normal and shear stresses, respectively, R_{in} and R_{out} refer to the inner and outer radii, respectively. Combining (1 - 3), a matrix depends only on h can be attained, which satisfies [11]:

$$\left[H_{ij}\right]_{4\times4}\begin{bmatrix}A\\B\\C\\D\end{bmatrix}=0, \tag{4}$$

where the value of each element in $[H]$ was given in [11]. To have the nontrivial solution, $\det[H_{ij}]_{4\times4}$ has to be zero. With h determined, the resonance frequency f_0 can be obtained via:

$$f_0=\frac{h}{2\pi}\sqrt{\frac{E}{\rho\left(1-\nu^2\right)}}, \tag{5}$$

where E and ρ refer to the Young's modulus and density. For simplification, f_0 cab be approximately expressed as:

$$f_0=\frac{1}{2\left(R_{out}-R_{in}\right)}\sqrt{\frac{E}{\rho}}. \tag{6}$$

Pursuant to (6), with ring width unchanged, R_{out} and R_{in} can be flexibly modified for larger transduction areas.

Nevertheless, despite the distinct advantage of EWGM, the conventional straight beam tether with higher stiffness and larger vibration amplitudes is detrimental to the EWGM resonators performance, especially at the UHF range. Herein a novel beam-frame mixing tether design was proposed, which reduces the equivalent stiffness, thus substantially alleviating the required bias voltages. Besides, the strain energy distributions can also be moderated to effectively suppress the anchor loss. As shown in Fig. 1(b), two tethers are located at the opposite quasi nodal regions.

B. Optimized tether design

A vibrating structure can be essentially characterized using a lumped model composed of a mass and a spring, thus, the resonators with tethers can be regarded as two serial springs, as shown in Fig. 2. The total equivalent stiffness of the device can be written as:

Fig. 2. The schematic of the serial springs.

$$\frac{1}{k_{eff}}=\frac{1}{k_{res}}+\frac{1}{k_{te}}, \tag{7}$$

where k_{res} and k_{te} refer to the equivalent stiffness of the resonating body and tethers, respectively. The k_{res} can be expressed as [13]:

$$k_{res}=\omega_0^2\frac{\rho h_{res}\int_0^{2\pi}\int_{R_{in}}^{R_{out}}\left(u_r\left(r,\theta\right)\right)^2 rdrd\theta}{\left(u_{r\_\max}\left(r,\theta\right)\right)^2}, \tag{8}$$

where h_{res} denotes the thickness of the resonator. Clearly, with the given mode shape, it is hard to reduce the stiffness of the resonating body. However, with the folded structure introduced in the tether, the tether stiffness can be significantly decreased [14]. According to (7), a lower total stiffness can thus be attained.

In addition, noting that Q is defined as the ratio of the total energy to the dissipations, the Q_{anchor} is proportional to the ratio of the stored strain energy in the whole device to the dissipated one through tethers [15]:

$$Q_{anchor}\propto\frac{E_{res}}{E_{te}}=\frac{\frac{1}{2}k_rX_r^2}{\frac{1}{2}k_tX_t^2}, \tag{9}$$

where E_{res}, E_{te}, k_r, k_t, X_r, and X_t are stored energies, stiffnesses, and vibration amplitudes of the resonator and tether, respectively. For conventional straight beam tether, optimizing beam dimensions can achieve very limited Q improvements. On the contrary, the mixing tether structure has lower stiffness, besides, with various tether geometries properly set, the displacement profile of the whole device can be optimized, thus achieving smaller vibrations. According to (9), a greatly improved Q_{anchor} value can be expected. In essence, the described tether design is flexible and feasible to achieve preferable strain energy distributions.

To obtain an optimal tether structure, as shown in Fig. 1(b), a finite element analysis (FEA) model has been established. The perfectly matched layers (PML) were employed to attenuate the

TABLE I. COMPARISON OF MECHANICAL PROPERTIES BETWEEN THE RESONATORS WITH CONVENTIONAL AND OPTIMIZED TETHERS

	Resonator types	
	Conventional tethers	***Optimized tethers***
k_{total} ($\times10^7$ N/m)	2.30	1.42
Q_{anchor} ($\times10^4$)	4.50	77.8

acoustic waves propagating in the substrate [16]. With the simulated displacement profile, the total stiffness of the whole device can be extracted using the following formula:

$$k_{eff} = \omega_0^2 \frac{\rho \int_{V_{EWGM}} \left(q(x,y,z)\right)^2 dV}{\left(q_{max}(x,y,z)\right)^2}, \quad (10)$$

where V_{EWGM} and $q(x, y, z)$ refer to the device volume and the displacement at an arbitrary point. Table 1 compares the stiffness of resonators with conventional and optimized tethers. Clearly, a nearly 40% k_{eff} reduction has been achieved. What's more, the simulated Q_{anchor} values increase from 4.50×10^4 to 7.78×10^5, corresponding to more than 17-fold enhancements. The simulations infer that the novel tether design enables significant performance improvement. It should be addressed that the simulated results just reflect the Q variation trend, which could be far beyond the actual results since other losses were not involved in the model.

C. Reduced Bias voltage

According to the capacitive transduction mechanism, the motional current i_{out} takes the form as :

$$i_{out} \propto Q \frac{A_0 V_P^2}{k_{eff} d_0^4}, \quad (11)$$

where A_0 and d_0 denote the transduction area and the spacing gap, respectively. As can be seen, the described resonator with enlarged transduction area, reduced mechanical stiffness, and improved Q values is apt to generate high motional current with lower bias voltage.

D. Fabrication

In addition to the above-mentioned optimizations in terms of the resonator design, shrinking the spacing gap is the most efficient method, which, however, imposes great challenges on the fabrication process. This work employs a simple and reliable silicon-on-insulator (SOI) process as described in [17], wherein the nano-scale spacing gap of 70 nm was employed, hence, V_P can be furthermore reduced. The SEM photographs of the fabricated resonators with conventional and optimized tethers are given in Fig. 3.

III. Results and Discussions

The resonators with two types of tether designs were tested on a RF probe station. As shown in Fig. 4, all the devices were vibrating at ultra-high frequencies over 548 MHz. In air, the resonator with conventional tethers had a smaller Q of 5500, while a high bias voltage of 17 V was needed (Fig. 4(a)). By

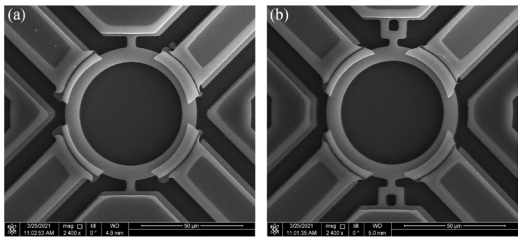

Fig. 3. The SEM photographs of the EWGM resonators with conventional (a) and optimized (b) tethers.

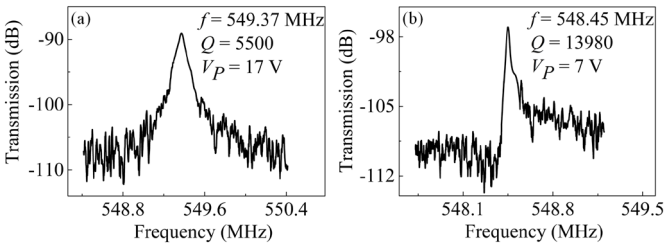

Fig. 4. Frequency responses of the EWGM resonators with conventional (a) and optimized (b) tethers in air.

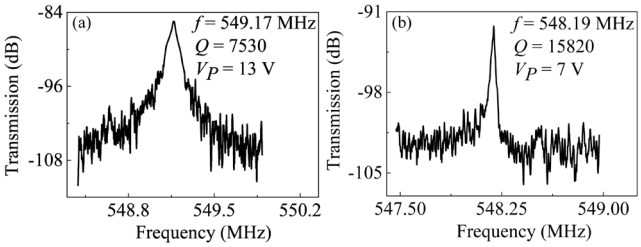

Fig. 5. Frequency responses of the EWGM resonators with conventional (a) and optimized (b) tethers in vacuum.

contrast, for the counterpart with optimized tether design, a promising Q of 13980 was attained, corresponding to a substantial Q enhancements of over 2.5 times. Besides, the resonator can be driven into vibration with a much lower V_P of 7 V (Fig. 4(b)). Obviously, the optimized tether effectively suppressed the anchor loss and reduced the bias voltages, in accordance with the theoretical results.

In vacuum, as shown in Fig. 5, the bias voltages of two types of resonators were 13 V and 7 V, corresponding to Q values of 7530 and 15820, respectively, inferring that the optimized device maintained notable advantages of lower bias voltages and higher Q values.

It is worth noting that both two types of resonators gained moderate Q improvements in vacuum. To explicitly characterize the squeezed-film damping of EWGM resonators, a fluid-solid coupling simulation model was built up, for which the governing equation takes a form as [18]:

$$P_a \nabla^2(\delta p) - \frac{12\eta_{eff}}{d_0^2} \frac{\partial(\delta p)}{\partial t} = \frac{12\eta_{eff} P_a}{d_0^3} \frac{du_r(R,\theta,t)}{dt}, \quad (12)$$

where δp, P_a, and $u_r(R, \theta, t)$ are the varied pressure, ambient pressure, and time-harmonic displacement at the circumference of the disk, respectively, η_{eff} denotes the effective viscosity. The varied pressure profile of EWGM is shown in Fig. 6, and the simulated Q_{SFD} value in air was 6.51×10^5.

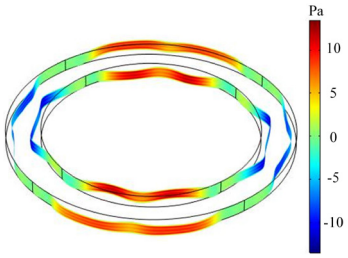

Fig. 6. The simulated varied pressure distribution of the EWGM resonator.

For the resonator with conventional tether design, the anchor loss plays a more important role in energy dissipations, which limits the Q enhancement. By contrast, for the counterpart with optimized tether design, the anchor loss has been dramatically reduced, however, with SFD effectively suppressed, the Q enhancement was still insignificant. There could be two reasons.

Firstly, the fabrication tolerances could induce slight mode distortions compared with the designed optimal one, which gives rise to more anchor loss. What's more, the Akhiezer damping resulting from the phonon-phonon interactions cannot be neglected. The Q_{AKE} is formulated as [19]:

$$Q_{AKE}=\frac{E_{eff}}{C_v T \gamma_{eff}^{\ 2}}\frac{1+\left(\omega_n \tau_{ph}\right)^2}{\omega_n \tau_{ph}}, \tag{13}$$

where C_v, and T denote the volumetric heat capability and ambient temperature, τ_{ph} denotes the relaxation time, E_{eff} and γ_{eff} refer to the effective bulk modulus and Grüneisen parameter, respectively, which are associated with the wave propagation directions [19]. For pure longitudinal and transverse waves, the Q_{AKE} values are calculated to be 1.15×10^5 and 7.83×10^4, respectively. For EWGMs, both P- and S-waves contribute to the Akhiezer damping, therefore, the orders of magnitude for the overall Q_{AKE} can be determined as 10^4, indicating that the Akhiezer damping overrides the anchor loss and squeezed film damping. As for thermoelastic damping (TED), it is generally negligible for BAW resonators [20].

Accordingly, for proposed EWGM resonators, the Akhiezer damping could be identified as a major limiting loss source. However, with some compensation methods, the fabrication tolerances induced mode shape distortions can be effectively eliminated, which is beneficial for a higher Q value. Besides, the air and vacuum tests infer that the proposed resonator is insusceptible to the air damping, which can alleviate the encapsulation requirements.

IV. Conclusions

In summary, a novel high-performance EWGM resonator with high Q values and low bias voltages was demonstrated. The optimized tether design with flexibility and feasibility was verified to simultaneously reduce the anchor loss and the mechanical stiffness, which paves the way to produce high-Q UHF resonators with lower bias voltages. The proposed resonators could have potential applications in building up high-end RF modules in future wireless communications.

Acknowledgment

This work was supported by the the National Key Research and Development Program of China (2018YFF01010300), the National Natural Science Foundation of China (61734007, 61804150), and the key research program of Frontier Science of CAS (QYZDY-SSW-JSC004).

References

[1] C. T.-C. Nguyen, "MEMS-based RF channel selection for true software-defined cognitive radio and low-power sensor communications," IEEE Commun. Mag., vol. 51, no. 4, pp. 110-119, 2013.

[2] D. Dubuc, K. Grenier, and J. Iannacci, "RF-MEMS for smart communication systems and future 5G applications," in Smart Sensors and MEMs: Elsevier, 2018, pp. 499-539.

[3] G. Wu, J. Xu, E. J. Ng, and W. Chen, "MEMS Resonators for Frequency Reference and Timing Applications," J. Microelectromech. Syst., vol. 29, no. 5, pp. 1137 - 1166, 2020.

[4] C. T.-C. Nguyen, "MEMS technology for timing and frequency control," IEEE Trans. Ultrason. Ferroelectr. Freq. Control, vol. 54, no. 2, pp. 251-270, 2007.

[5] T. L. Naing, T. O. Rocheleau, Z. Ren, S.-S. Li, and C. T.-C. Nguyen, "High-Q UHF Spoke-Supported Ring Resonators," J. Microelectromech. Syst., vol. 25, no. 1, pp. 11-29, 2015.

[6] M. Rinaldi, C. Zuo, J. Van der Spiegel, and G. Piazza, "Reconfigurable CMOS oscillator based on multifrequency AlN contour-mode MEMS resonators," IEEE Trans. Electron Devices, vol. 58, no. 5, pp. 1281-1286, 2011.

[7] A. Ozgurluk, M. Akgul, and C. T.-C. Nguyen, "RF Channel-Select Micromechanical Disk Filters—Part I: Design," IEEE Trans. Ultrason. Ferroelectr. Freq. Control, vol. 66, no. 1, pp. 192-217, 2019.

[8] J. R. Clark, W.-T. Hsu, M. A. Abdelmoneum, and C.-C. Nguyen, "High-Q UHF micromechanical radial-contour mode disk resonators," J. Microelectromech. Syst., vol. 14, no. 6, pp. 1298-1310, 2005.

[9] S. Pourkamali, G. K. Ho, and F. Ayazi, "Low-impedance VHF and UHF capacitive silicon bulk acoustic-wave resonators—Part II: Measurement and characterization," IEEE Trans. Electron Devices, vol. 54, no. 8, pp. 2024-2030, 2007.

[10] J. Wang, Z. Ren, and C.-C. Nguyen, "1.156-GHz self-aligned vibrating micromechanical disk resonator," IEEE Trans. Ultrason. Ferroelectr. Freq. Control, vol. 51, no. 12, pp. 1607-1628, 2004.

[11] T. Takano, H. Hirata, and Y. Tomikawa, "Analysis of nonaxisymmetric vibration mode piezoelectric annular plate and its application to an ultrasonic motor," IEEE Trans. Ultrason. Ferroelectr. Freq. Control, vol. 37, no. 6, pp. 558-565, 1990.

[12] Y. Xie, S.-S. Li, Y.-W. Lin, Z. Ren, and C. T.-C. Nguyen, "1.52-GHz micromechanical extensional wine-glass mode ring resonators," IEEE Trans. Ultrason. Ferroelectr. Freq. Control, vol. 55, no. 4, pp. 890-907, 2008.

[13] M. Akgul, L. Wu, Z. Ren, and C. T.-C. Nguyen, "A negative-capacitance equivalent circuit model for parallel-plate capacitive-gap-transduced micromechanical resonators," IEEE Trans. Ultrason. Ferroelectr. Freq. Control, vol. 61, no. 5, pp. 849-869, 2014.

[14] X. Lv, W. Wei, X. Mao, J. Yang, and F. Yang, "A novel MEMS actuator with large lateral stroke driven by Lorentz force," J. Micromech. Microeng., vol. 25, no. 2, p. 025009, 2015.

[15] J. E. Lee, J. Yan, and A. A. Seshia, "Study of lateral mode SOI-MEMS resonators for reduced anchor loss," J. Micromech. Microeng., vol. 21, no. 4, p. 045010, 2011.

[16] V. Thakar and M. Rais-Zadeh, "Optimization of tether geometry to achieve low anchor loss in Lamé-mode resonators," in 2013 Joint European Frequency and Time Forum & International Frequency Control Symposium (EFTF/IFC 2013), 2013, pp. 129-132: IEEE.

[17] Z. Chen et al., "A Novel Lamé Mode RF-MEMS Resonator with High Quality Factor," Int. J. Mech. Sci., p. 106484, 2021.

[18] M. Bao and H. Yang, "Squeeze film air damping in MEMS," Sens. Actuator A-Phys., vol. 136, no. 1, pp. 3-27, 2007.

[19] S. S. Iyer and R. N. Candler, "Mode-and direction-dependent mechanical energy dissipation in single-crystal resonators due to anharmonic phonon-phonon scattering," Phys. Rev. Appl., vol. 5, no. 3, p. 034002, 2016.

[20] R. Abdolvand, B. Bahreyni, J. Lee, and F. Nabki, "Micromachined resonators: A review," Micromachines, vol. 7, no. 9, p. 160, 2016.